PHYSICS OF FLUIDS **28**, 053305 (2016)

Multi-dimensional rheology-based two-phase model for sediment transport and applications to sheet flow and pipeline scour

Cheng-Hsien Lee,[1,2] Ying Min Low,[1,a)] and Yee-Meng Chiew[3]
[1]*Centre for Offshore Research and Engineering, Department of Civil and Environmental Engineering, National University of Singapore, 1 Engineering Drive 2, Singapore 117576, Singapore*
[2]*Department of Water Resources and Environmental Engineering, Tamkang University, New Taipei City 25137, Taiwan*
[3]*School of Civil and Environmental Engineering, Nanyang Technological University, Singapore*

(Received 3 November 2015; accepted 28 April 2016; published online 24 May 2016)

Sediment transport is fundamentally a two-phase phenomenon involving fluid and sediments; however, many existing numerical models are one-phase approaches, which are unable to capture the complex fluid-particle and inter-particle interactions. In the last decade, two-phase models have gained traction; however, there are still many limitations in these models. For example, several existing two-phase models are confined to one-dimensional problems; in addition, the existing two-dimensional models simulate only the region outside the sand bed. This paper develops a new three-dimensional two-phase model for simulating sediment transport in the sheet flow condition, incorporating recently published rheological characteristics of sediments. The enduring-contact, inertial, and fluid viscosity effects are considered in determining sediment pressure and stresses, enabling the model to be applicable to a wide range of particle Reynolds number. A $k-\varepsilon$ turbulence model is adopted to compute the Reynolds stresses. In addition, a novel numerical scheme is proposed, thus avoiding numerical instability caused by high sediment concentration and allowing the sediment dynamics to be computed both within and outside the sand bed. The present model is applied to two classical problems, namely, sheet flow and scour under a pipeline with favorable results. For sheet flow, the computed velocity is consistent with measured data reported in the literature. For pipeline scour, the computed scour rate beneath the pipeline agrees with previous experimental observations. However, the present model is unable to capture vortex shedding; consequently, the sediment deposition behind the pipeline is overestimated. Sensitivity analyses reveal that model parameters associated with turbulence have strong influence on the computed results. *Published by AIP Publishing.* [http://dx.doi.org/10.1063/1.4948987]

I. INTRODUCTION

The particles in sediment transport may be suspended in the flow (suspended load) or move on the bed (bed load). A range of numerical models is available for computing the transport of sediments. Most of these models are single-phase approaches[1,2] in which the sediments suspended in flows are regarded as a passive scalar and the bed-load transport rate is computed using published empirical formulas.[3–5] In reality, sediment transport is a two-phase phenomenon, where the sediment is the dispersed phase and the fluid is the carrier phase; thus, single-phase approaches cannot fully capture the fluid-sediment interactions.

a)Author to whom correspondence should be addressed. Electronic mail: ceelowym@nus.edu.sg. Tel.: +65 65164127. Fax: +65 67791635.

The limitation of single-phase approaches has led to the development of two-phase models in the last decade.[6–13] In the two-phase models, both the sediment and fluid have their own governing equations for mass and momentum with the latter incorporating terms to describe the momentum interchange (interfacial forces). The main differences between these models are how the stresses of the sediment and fluid phases are determined.

The Reynolds stresses, associated with turbulence, are the most important part of the fluid stresses. The eddy-viscosity (turbulent-viscosity) hypothesis[14] is used in the two-phase models. Some studies[9,10,13,15] further use the mixing length approach to compute the eddy viscosity. In clear water conditions, the mixing length is only associated with the distance to a boundary.[14] Li and Sawamoto[13] extended the mixing length model in clear water to sediment transport problems by incorporating the effect of the sediment concentration, which was adopted by Revil-Baudard and Chauchat.[9] Chiodi *et al.*[15] proposed a differential equation that incorporates the local Reynolds number to compute the mixing length. The main drawback of the mixing length models is their limitation to one-dimensional (1D) problems. Other studies[6–13,16] use the $k-\epsilon$ model to compute the eddy viscosity, where k is the turbulence kinetic energy and ϵ is its dissipation rate. The $k-\epsilon$ models are similar to that used for clear water problems, but they include various effects of sediment on turbulence modulation, such as (1) the dissipation of turbulence due the correlation of fluctuation velocities of sediment and fluid and (2) the buoyance production of turbulence due to the sediment concentration gradient.[6] Chen *et al.*[12] do not incorporate both effects.

The sediment stresses reflect the individual interaction of sediment particles. Microscopically, sediment particles can manifest three effects; namely, enduring contact, mutual collision (inertial), and fluid viscous effects on sediment interactions. These three effects yield distinct different rheological characteristics on the sediments. The enduring-contact effect yields the Coulomb relationship, that is, stresses are independent of strain rates.[17] The inertial effect leads to stresses depending on the square of the strain rates, and the viscous effect results in stresses associated with the strain rates.[18] The enduring-contact effect plays an important role only for very high concentration flows.[19,20] The inertial and fluid viscous effects have an inverse relationship. The relative importance of inertia and viscosity is associated with the particle Reynolds number, $\mathrm{Re}_* = u_* d/\nu_f$, where u_* = the shear velocity, d = the particle diameter, and ν_f = the kinematic viscosity of fluid.[18] Fluid viscosity dominates when $\mathrm{Re}_* < 10$ while inertia is dominant when $\mathrm{Re}_* > 55$; in between, both the effects are important. Previous studies[6–8] considered the inertial effect by using the sediment stress derived from granular kinetic theories and the enduring-contact effect, but fluid viscosity was neglected. Other studies[12,16,21] accounted for only the viscosity using the closures of sediment stress obtained experimentally. Recently, Chiodi *et al.*[15] and Revil-Baudard and Chauchat[9] incorporated all three effects in their models based on recent findings of rheological characteristics of sediments.[22,23]

Most two-phase models are confined to 1D problems, except for the 2D models of Amoudry and Liu[24] and Yeganeh-Bakhtiary *et al.*,[21] which are based on $k-\epsilon$ models to compute the Reynolds stress. In modeling the sediment stress, Amoudry and Liu[24] considered the inertial and enduring-contact effects, whereas Yeganeh-Bakhtiary *et al.*[21] considered only the viscous effect. Both models are based on the Cartesian grid system, so that their applications are restricted to flow problems with simple geometries. Besides, the two models assume that the sediment particles are static within the sand bed; hence, the two models cannot simulate avalanches in which there is a sediment movement not only on the surface but also inside the sand bed when the bed slope exceeds a critical value.

To overcome some of the limitations of existing numerical models, this paper develops a multi-dimensional two-phase model that supports unstructured grid systems and considers the enduring-contact, inertial, and fluid viscous effects. In this model, the sediments within the sand bed are not assumed to be static. The governing equations in the proposed model are solved using OpenFOAM®, an open source computational-fluid-dynamics library. Although OpenFOAM® provides a two-phase solver, namely, "twoPhaseEulerFoam", it cannot predict the fluid pore pressure and sediment pressure correctly, thus the proper angle of repose cannot be reproduced.[25] Recently, Lee *et al.*[25] have proposed a new numerical scheme for dry granular materials that can accurately

predict the angle of repose. Here, the numerical scheme is extended to two-phase flow problems to simulate sheet flow and scour around a submarine pipeline.

II. MATHEMATICAL FORMULATION

A. Governing equations

Macroscopic equations governing the two phases can be obtained by taking averages over the microscopic governing equations for each phase (e.g., Navier-Stokes equations for fluids).[26] Since the macroscopic motion of fluid and sediment for a large-scale flow may still include large-scale turbulent fluctuations, some previous studies[27] suggest applying other averaging operations over the original macroscopic equations. If Favre averaging (concentration-weighted averaging) is chosen, the governing equations of mass and momentum for the fluid and sediment phases read[27]

$$\frac{\partial \rho_f (1-c)}{\partial t} + \nabla \cdot \left[\rho_f (1-c)\,\mathbf{u}^f\right] = 0 \tag{1}$$

$$\frac{\partial \rho_f (1-c)\,\mathbf{u}^f}{\partial t} + \nabla \cdot \left[\rho_f (1-c)\,\mathbf{u}^f\mathbf{u}^f\right] = \rho_f (1-c)\,\mathbf{g} - (1-c)\,\nabla p_f + \nabla \cdot (1-c)\,\mathbf{T}^f - \left\{ c\rho_s \frac{\mathbf{u}^f - \mathbf{u}^s}{\tau_p} - \frac{\rho_s}{\tau_p}\frac{(1-c)\,\nu_{ft}}{\sigma_c}\nabla c \right\} \tag{2}$$

and

$$\frac{\partial \rho_s c}{\partial t} + \nabla \cdot (\rho_s c \mathbf{u}^s) = 0 \tag{3}$$

$$\frac{\partial \rho_s c \mathbf{u}^s}{\partial t} + \nabla \cdot (\rho_s c \mathbf{u}^s \mathbf{u}^s) = \rho_s c \mathbf{g} - c\nabla p_f - \nabla (c p_s) + \nabla \cdot c\mathbf{T}^s + \left\{ c\rho_s \frac{\mathbf{u}^f - \mathbf{u}^s}{\tau_p} - \frac{\rho_s}{\tau_p}\frac{(1-c)\,\nu_{ft}}{\sigma_c}\nabla c \right\}, \tag{4}$$

where ρ_f and ρ_s are the mass densities of the fluid and sediment phases, respectively; c is the averaged sediment volume concentration; $\mathbf{u}^f$ and $\mathbf{u}^s$ are the concentration-weighted mean velocities of the fluid and sediment phases, respectively; $\mathbf{g}$ is the acceleration due to gravity; p_f is the static pressure of fluid phase; p_s is the pressure of sediment phase; $\mathbf{T}^f$ and $\mathbf{T}^s$ are stresses of the fluid and sediment phases, respectively. The two terms in { } in Eqs. (2) and (4) refer to the interphase momentum transfer. Of these two terms, $c\rho_s(\mathbf{u}^f - \mathbf{u}^s)/\tau_p$ accounts for the drag force (where τ_p is the particle response time relating to drag coefficient) while $\rho_s (1-c)\,\nu_{ft}\nabla c/\tau_p\sigma_c$ (where ν_{ft} is the eddy viscosity of fluid phase and σ_c is the Schmidt number) arises from the averaging process and accounts for turbulent dispersion that causes sediment transport from a high to low concentration region. Following previous studies,[6] τ_p is calculated as follows:

$$\tau_p = \frac{\rho_s}{\rho_f \nu_f d^2}\frac{(1-c)^n}{(18 + 0.3\mathrm{Re}_p)}, \tag{5}$$

where ν_f = the kinematic viscosity of fluid, $Re_p = U_r d/\nu_f$ with $U_r = \left|\mathbf{u}^f - \mathbf{u}^s\right|$, and $n = 4.45\mathrm{Re}_p^{-1}$. In contrast to incompressible flow for fluids, Eqs. (1) and (3) indicate that the velocity field is not divergence free due to the presence of sediments.

Equations (1)-(5) involves 31 variables (such as ρ_s, ρ_f, c, ν_{ft}, σ_c, p_s, p_f, $\mathbf{u}^f$, $\mathbf{u}^s$, $\mathbf{T}^s$, and $\mathbf{T}^f$), and proper closure models or constitutive equations are required to solve the problems defined by therein. Proper closure models should reflect their corresponding microscopic behaviors. This study assumes that the fluid and sediments are incompressible, i.e., ρ_f and ρ_s are constants. The viscous stresses, $\mathbf{T}^{fv}$, and the Reynolds stresses, $\mathbf{T}^{ft}$, are considered when computing $\mathbf{T}^f$, that is,

$$\mathbf{T}^f = \mathbf{T}^{fv} + \mathbf{T}^{ft}. \tag{6}$$

Most of the previous studies[6–8,27] suggested modifying a standard $k-\epsilon$ model (for clear water) to compute $\mathbf{T}^{ft}$. However, the standard $k-\epsilon$ model cannot be applied to regions near the bed with low Reynolds number. Launder and Sharma[28] proposed a low-Reynolds-number correction for the standard $k-\epsilon$ model. Herein, a $k-\epsilon$ model similar to that of Hsu *et al.*[6] but with

low-Reynolds-number correction is adopted to compute $\mathbf{T}^{ft}$. Details of the computation of $\mathbf{T}^{fv}$ and $\mathbf{T}^{ft}$ are provided in the Appendix. Moreover, $\mathbf{T}^s$ is computed according to: (1) recent finding of rheological characteristics of granular martial in fluid;[22,23,29] and (2) analytical results of turbulent motion of sediment in turbulent flows,[30] which is described next.

B. Constitutive equations for the sediment stresses

The rheological characteristics of sediment are first discussed. The enduring contact, sediment inertia, and fluid viscosity all have effects on the rheological characteristics. If fluid viscosity is negligible, the rheology of sediment can be described by friction and dilatancy laws that depend on the inertial number[31]

$$I_i = \frac{2dD^s}{\sqrt{cp_s d/\rho_s}}, \tag{7}$$

where D^s is the second invariant of the strain rate, $\mathbf{D}^s = \left[\nabla\mathbf{u}^s + (\nabla\mathbf{u}^s)^T\right]/2$. The inertial number ($I_i$) is equivalent to the Savage number,[32] which describes the ratio of inertial shear stress to quasi-static stress associated with the weight (resulting from enduring contact). If fluid viscosity is pronounced, the kinetic energy of sediment particles will be damped by fluid viscosity and the fall velocity is reduced; in this situation, the inertia effect is insignificant, and friction and dilatancy behaviors depend on another dimensionless parameter[23]

$$I_\nu = \frac{2\rho_f \nu_f D^s}{cp_s d}, \tag{8}$$

which is equivalent to the friction number[32] defined by the ratio of the viscous shear stress to the stress associated with the weight. The relative importance of fluid viscosity to sediment inertia can be measured by the Stokes number[22]

$$\mathrm{St} = \frac{I_i^2}{I_\nu} = \frac{\rho_s D^s d^2}{\nu_f}. \tag{9}$$

Sediment inertia is important when $\mathrm{St} \gg 1$, conversely fluid viscosity is dominant for $\mathrm{St} \ll 1$. The Stokes number is similar to the Bagnold number[18] defined as the ratio of the inertial grain stress to the viscous shear stress. The particle Reynolds number (Re_*) can also be used to characterize this ratio. Because Re_* depends on shear velocity (a global property) and St depends on a local shear rate, Re_* and St are, respectively, suitable for global and local characterization.

Recently, Trulsson *et al.*[22] found that the rheological characteristics, incorporating the enduring-contact, inertial, and the fluid viscous effects, can be well characterized by a dimensionless parameter combining I_i and I_ν

$$I = I_\nu + aI_i^2, \tag{10}$$

where a is a constant. Here, I is used to describe the rheological characteristics. Equations (9) and (10) indicate that when $\mathrm{St} > 1/a$, inertia becomes more important than fluid viscosity. According to Bagnold[18] when $\mathrm{St}/[(c_{rcp}/c)^{1/3} - 1]^{1/2}$ (where c_{rcp} = random close packing fraction) exceeds a value around $40 - 150$, inertia will dominate; this suggests that $a \approx 0.01 - 0.11$ when $0.1 < c < 0.55$. In this study, $a = 0.11$ is adopted.

It is assumed that the dilatancy law can be described by

$$c = \frac{c_c}{1 + bI^{1/2}}, \tag{11}$$

where c_c is the critical concentration and b is a model parameter. Equation (11) reduces to the dilatancy law of Boyer *et al.*[23] for viscous-dominated flow when $b = 1$ and St is very small. Herein, $b = 1$ and $c_c = 0.62$ are adopted; $c_c = 0.62$ is between the random close packing fraction ($\approx$0.64) and the random loose packing fraction ($\approx$0.58).

Trulsson *et al.*[22] proposed the frictional law that depends on I

$$\eta = \eta_1 + \frac{\eta_2 - \eta_1}{1 + I_o/I^{1/2}}, \tag{12}$$

where $\eta = T^s/p_s$ with T^s being the second invariant of $\mathbf{T}^s$, $\eta_1 = \tan\theta_s$ with θ_s = the angle of repose, and η_2 as well as I_o is a constant. This study uses $\eta_2 = 0.82$, obtained experimentally,[33] and $I_o = 0.1$ obtained numerically.[22] When I approaches zero, Eq. (12) reduces to the Coulomb relationship (T^s/p_s = constant); moreover, η increases with I; consequently, Eq. (12) describes a viscoplastic behavior. When St is very large (viscosity is negligible), Eq. (12) reduces to the frictional law of Jop *et al.*[31] for dry granular material.

It is noted that Eqs. (11) and (12) neglect the effect of fluid turbulence on sediment stresses; in addition, Eq. (11) also neglects the elastic behavior of sediment, which is important when sediment is in the static state. To take into account the rheological characteristics described by Eqs. (11) and (12), the effect of fluid turbulence and the elastic behavior p_s is herein divided into three components

$$p_s = p_{sr} + p_{se} + p_{st}, \tag{13}$$

where p_{sr} reflects the rheological characteristics when sediment moves, p_{se} accounts for the elastic effect when sediment is static, and p_{st} accounts for the turbulent motion of sediment particles. According to Eqs. (7), (8), (10), and (11), p_{sr} is evaluated as

$$p_{sr} = \frac{2b^2 c}{d(c_c - c)^2}\left(\rho_f \nu_f + 2a\rho_s d^2 D^s\right) D^s. \tag{14}$$

The formula proposed by Hsu *et al.*[6] is adopted here to compute p_{se}

$$p_{se} = K[\max(c - c_o, 0)]^\chi \left\{1 + \sin\left[\max\left(\frac{c - c_o}{c_{rcp} - c_o}\right)\pi - \frac{\pi}{2}\right]\right\}, \tag{15}$$

where c_{rcp} = random close packing fraction, and c_o, K, and χ are the model parameters. Obviously, K is related to the granular material's Young's modulus and the other terms are associated with material deformation. Lee *et al.*[25] suggested $K = 10^8$ Pa and $\chi = 1.5$ for a problem of collapsing granular column, and these values are adopted here, resulting in the concentration in the sand bed being close to c_o, which typically ranges from 0.58 to 0.64. Here, $c_o = 0.6$ is used. Similar to the fluid phase, p_{st} is related to the fluctuating motion. An analysis of heavy and small particles in a homogeneous steady turbulent flow[30] suggests that the square of fluctuating velocity of sediment equals αk where α is given by Eq. (A5); thus, p_{st} can be expressed as

$$p_{st} = \frac{2}{3}\rho_s \alpha k. \tag{16}$$

The shear stress for the sediment phase can be written as

$$\mathbf{T}^s = \left(-\frac{2}{3}\rho_s \nu_s \nabla \cdot \mathbf{u}^s\right)\mathbf{I} + 2\rho_s \nu_s \mathbf{D}^s, \tag{17}$$

where ν_s is the kinematic viscosity. Both the viscoplastic behavior (Eq. (12)) and turbulence behavior are considered, hence ν_s is divided into two components

$$\nu_s = \nu_{sv} + \nu_{st}, \tag{18}$$

where ν_{sv} and ν_{st} represent the viscoplastic and turbulence effects, respectively. Using a regularization technique[34] and invoking Eq. (12), ν_{sv} is given by

$$\nu_{sv} = \frac{(p_{sr} + p_{se})\eta}{2\rho_s D^s}. \tag{19}$$

Equation (19) considers sediment in the static state to be a very viscous fluid. For computing ν_{st}, previous studies[30] suggested that

$$\nu_{st} = \alpha \nu_{ft} \tag{20}$$

after analyzing the behavior of heavy and small particles in homogeneous steady turbulent flow.

In order to span the various sediment transport regimes, this study combines the constitutive relations that are applicable to compacted bed, dense flows, and dilute suspensions. When $c \ll c_0$ (i.e., dilute suspensions), $p_{sr} \to 0$, $p_{se} \to 0$, and $\nu_{sv} \to 0$. Only turbulence contributions (p_{st} and ν_{st}) are crucial. For $c > c_o$, the previous study of Lee *et al.*[25] suggests that this region belongs to compacted bed, where sediment is in the static state and no turbulent motion of fluid exists; hence, only the elasticity contribution (p_{se}) is important. For dense flow, both the turbulent and viscoplastic (or rheological) contributions are influential in which case the aggregation effect may be significant, and it is much more subtle to assign appropriate values for the coefficients of the constitutive models. This aggregation effect may be a possible source of discrepancy between the numerical and experimental results.

C. Rheological characteristics

As mentioned in Section II B, the $c - I$ relationship (Eq. (11)) can only reduce to $c = c_c/(1 + I_v^{1/2})$ for small St. For large St, this relationship can be expressed by Ref. 35

$$c = c_c - 0.1 I_i. \tag{21}$$

Similarly, the $\eta - I$ relationship (Eq. (12)) can only reduce to $\eta = \eta_1 + (\eta_2 - \eta_1)/(1 + I_o/a^{1/2} I_i)$[31] for large st. For small st, η is given by Boyer *et al.*[23]

$$\eta = \eta_1 + \frac{\eta_2 - \eta_1}{1 + I_{vo}/I_v}, \tag{22}$$

where $I_{vo} = 0.005$ is a model parameter and $\eta_1 = 0.43$ (typical for glass beads).[33] To check the applicability of Eqs. (11) and (12) for large and small St, respectively, Fig. 1 compares Eq. (11) against Eq. (21) and compares Eq. (12) against Eq. (22). It can be seen in Fig. 1 that Eqs. (11) and (12) have similar behavior with Eqs. (21) and (22), respectively. Hence, Eqs. (11) and (12) may be applied for St from small to large values.

D. Summary

This section has presented the mathematical formulas of a new two-phase model for sediment transport, where key parameters are summarized in Table I. The two parameters, η_1 and $C_{\epsilon 3}$, are not included in Table I because η_1 depends on the angle of repose and varies with different sediment particles, whereas $C_{\epsilon 3}$ is associated with influence of sediment on turbulence and is usually calibrated empirically. The former depends on the angle of repose and it is different for different sediment particles; the latter is associated with influence of sediment on turbulence and it is usually calibrated to yield good agreement with a particular laboratory experiment.[36] The present model

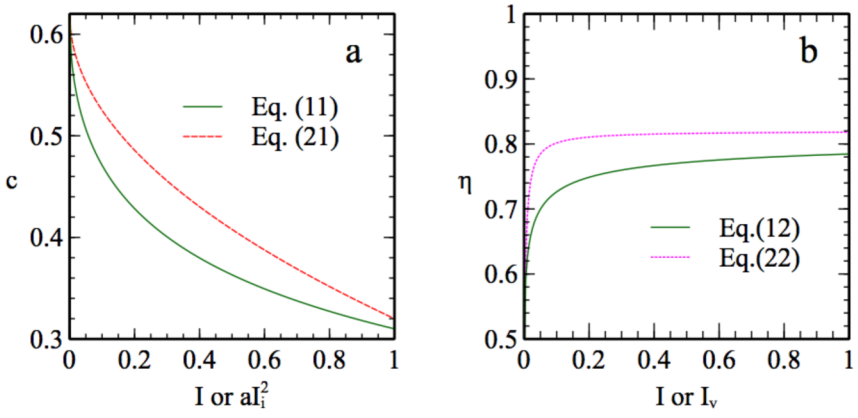

FIG. 1. Plot of c against I or aI_i^2 (a) and η against I or I_v (b).

TABLE I. Model parameters used in this study.

a	b	I_o	η_2	c_o
0.11	1	0.1	0.82	0.6
c_c	c_{crp}	K	χ	C_μ
0.62	0.64	10^8 Pa	1.5	0.09
$C_{\epsilon 1}$	$C_{\epsilon 2}$	σ_k	σ_ϵ	σ_c
1.44	1.92	1	1.3	1

has some similarities to some recently developed models,[9,15] which are also based on the recently discovered rheological characteristics of sediments. The present and recently developed models consider the sediment inertia and fluid viscosity effects so that a wide range of Re_* is applicable. The present model distinguishes itself from previous ones[9,15] in that the Reynolds stress is calculated using a $k-\epsilon$ model with low-Reynolds number correction, whereas previous models are based on the zero-equation mixing-length approach. Moreover, the present model can be applied to solve multi-dimensional problems but previous models are limited to 1D problems. In contrast to other multi-dimensional models[21,24] as mentioned in Section I, the present model fully considers the interaction of sediments in fluids.

III. NUMERICAL SCHEME

This study uses OpenFOAM® to solve the governing and constitutive equations presented in Section II. OpenFOAM® allows code developers to sidestep the discretization of derivative terms. However, there remains the challenge of avoiding the numerical instability caused by high sediment concentration, which may induce infinite pressure (see Eq. (14)). A new solution procedure has been outlined to solve such equations and avoid numerical instability by extending the solution procedure proposed by Lee *et al.*[25] for simulating dry granular flows. Subsequently, one can avoid dividing the computational domain into two regions: inside and outside the sand bed, which is difficult to implement in an unstructured system.

A. Semi-discretized forms of the governing equations

To avoid numerical noises occurring when $c \to 0$, the momentum equations (Eqs. (2) and (4)) are divided by $\rho_f(1-c)$ and $\rho_s c$ and solved in the "phase-intensive" form as suggested by Rusche[37]

$$\frac{\partial \mathbf{u}^f}{\partial t} + \nabla\cdot\left(\mathbf{u}^f\mathbf{u}^f\right) - \left(\nabla\cdot\mathbf{u}^f\right)\mathbf{u}^f = \mathbf{g} - \frac{1}{\rho_f}\nabla p_f + \frac{1}{\rho_f}\nabla\cdot\mathbf{T}^f - \mathbf{T}^f\cdot\frac{\nabla c}{\rho_f(1-c)} - \frac{c\rho_s}{\rho_f(1-c)}\frac{\left(\mathbf{u}^f-\mathbf{u}^s\right)}{\tau_p} + \frac{\rho_s}{\rho_f(1-c)\tau_p}\frac{\nu_{ft}}{\sigma_c}\nabla c \tag{23}$$

and

$$\frac{\partial \mathbf{u}^s}{\partial t} + \nabla\cdot\left(\mathbf{u}^s\mathbf{u}^s\right) - \left(\nabla\cdot\mathbf{u}^s\right)\mathbf{u}^s = \mathbf{g} - \frac{1}{\rho_s}\nabla p_f - \frac{1}{\rho_s c}\nabla c p_s + \frac{1}{\rho_s}\nabla\cdot\mathbf{T}^s + \mathbf{T}^s\cdot\frac{\nabla c}{\rho_s c} + \frac{\left(\mathbf{u}^f-\mathbf{u}^s\right)}{\tau_p} - \frac{1}{c\tau_p}\frac{\nu_{ft}}{\sigma_c}\nabla c. \tag{24}$$

The solutions of Eqs. (23) and (24) are expressed in the semi-discretized forms

$$\mathbf{u}^f = \frac{\mathbf{A}_H^f}{\mathbf{A}_D^f} + \frac{\mathbf{g}}{\mathbf{A}_D^f} - \frac{\nabla p_f}{\rho_f\mathbf{A}_D^f} + \frac{\rho_s c\mathbf{u}^s}{\rho_f\mathbf{A}_D^f(1-c)\tau_p} + \frac{\rho_s}{\rho_f\mathbf{A}_D^f(1-c)\tau_p}\frac{\nu_{ft}}{\sigma_c}\nabla c \tag{25}$$

$$\mathbf{u}^s = \frac{\mathbf{A}_H^s}{\mathbf{A}_D^s} + \frac{\mathbf{g}}{\mathbf{A}_D^s} - \frac{\nabla p_f}{\rho_s \mathbf{A}_D^s} - \frac{\nabla p_s}{\rho_s \mathbf{A}_D^s} - \frac{p_s \nabla c}{\rho_s \mathbf{A}_D^s c} + \frac{\rho_s \mathbf{u}^f}{\mathbf{A}_D^s \tau_p} - \frac{1}{\mathbf{A}_D^s c \tau_p} \frac{\nu_{ft}}{\sigma_c} \nabla c, \tag{26}$$

where $\mathbf{A}^w$ ($w = s$ or f) denotes the systems of linear algebraic equations arising from either the discretization of Eq. (23) or that of Eq. (24). The matrix $\mathbf{A}^w$ is decomposed into a diagonal matrix, $\mathbf{A}_D^w$, and an off-diagonal matrix, $\mathbf{A}_O^w$. Also, $\mathbf{A}_H^w = \mathbf{b}^w - \mathbf{A}_O^w \mathbf{u}^{\mathbf{w}}$ with $\mathbf{b}^w$ relating to the second to final terms on RHS of either Eqs. (25) and (26). OpenFOAM® built-in functions are used to compute $\mathbf{A}_D^w$ and $\mathbf{A}_H^w$, which depend on the discretization schemes. This study adopts a second-order time-implicit scheme and a limited linear interpolation scheme for all variables except for velocity.

B. A prediction-correction method

A novel prediction-correction method is proposed to compute $\mathbf{u}^f$ and $\mathbf{u}^s$; here, $\mathbf{u}^s$ is calculated first for numerical stability. Moreover, for numerical stability, it is beneficial to split Eq. (26) into a predictor

$$\mathbf{u}^{s'} = \frac{\mathbf{A}_H^s}{\mathbf{A}_D^s} + \frac{\mathbf{g}}{\mathbf{A}_D^s} - \frac{\nabla p_f}{\rho_s \mathbf{A}_D^s} - \frac{\nabla p_s}{\rho_s \mathbf{A}_D^s} + \frac{\rho_s \mathbf{u}^f}{\mathbf{A}_D^s \tau_p} \tag{27}$$

and a corrector term

$$\mathbf{u}^s = \mathbf{u}^{s'} - \left(\frac{p_s}{\rho_s \mathbf{A}_D^s c} + \frac{1}{\mathbf{A}_D^s c \tau_p} \frac{\nu_{ft}}{\sigma_c} \right) \nabla c. \tag{28}$$

Combining Eqs. (3) and (28) results in the following equation describing the evolution of c:

$$\frac{\partial c}{\partial t} + \nabla \cdot \left(c \mathbf{u}^{s'} \right) = \nabla \cdot \left(\frac{p_s}{\rho_s \mathbf{A}_D^s c} + \frac{1}{\mathbf{A}_D^s c \tau_p} \frac{\nu_{ft}}{\sigma_c} \right) \nabla c. \tag{29}$$

The RHS of Eq. (29) has a diffusive nature. Since p_s is large when sediment concentration is high, the RHS of Eq. (29) avoids a rapid increase of c and the instability caused by high sediment concentration. If Eq. (26) is directly used to calculate $\mathbf{u}^s$ and Eq. (3) to calculate c, then c may increase rapidly toward c_c, leading to an infinite p_s for large c.

For velocity-pressure coupling, Eq. (25) is similarly divided into a predictor

$$\mathbf{u}^{f*} = \frac{\mathbf{A}_H^f}{\mathbf{A}_D^f} + \frac{\mathbf{g}}{\mathbf{A}_D^f} + \frac{\rho_s c \mathbf{u}^s}{\rho_f \mathbf{A}_D^f (1-c) \tau_p} + \frac{\rho_s}{\rho_f \mathbf{A}_D^f (1-c) \tau_p} \frac{\nu_{ft}}{\sigma_c} \nabla c \tag{30}$$

and a corrector term

$$\mathbf{u}^f = \mathbf{u}^{f*} - \frac{\nabla p_f}{\rho_f \mathbf{A}_D^f}. \tag{31}$$

Eq. (31) can be directly substituted into Eq. (1) and a pressure equation is obtained; however, numerical experiments solving this pressure equation to simulate air-water flow have shown that the lighter material is poorly conserved.[38] To avoid poor conservation of lighter material, Carver[39] suggests combining Eqs. (1) and (3) into

$$\nabla \cdot \left[(1-c) \mathbf{u}^f + c \mathbf{u}^s \right] = 0 \tag{32}$$

and using Eq. (29) to correct p_f. In the spirit of Carver,[39] we define

$$\mathbf{u}^{s*} = \frac{\mathbf{A}_H^s}{\mathbf{A}_D^s} + \frac{\mathbf{g}}{\mathbf{A}_D^s} - \frac{\nabla p_s}{\rho_s \mathbf{A}_D^s} - \frac{p_s \nabla c}{\rho_s \mathbf{A}_D^s c} + \frac{\rho_s \mathbf{u}^f}{\mathbf{A}_D^s \tau_p} - \frac{1}{\mathbf{A}_D^s c \tau_p} \frac{\nu_{ft}}{\sigma_c} \nabla c \tag{33}$$

and combine Eqs. (26) and (31)–(33), yielding

$$\nabla \cdot \left[(1-c) \mathbf{u}^{f*} + c \mathbf{u}^{s*} \right] = \nabla \cdot \left[\frac{1-c}{\rho_f \mathbf{A}_D^f} + \frac{c}{\rho_s \mathbf{A}_D^s} \right] \nabla p_f. \tag{34}$$

The numerical scheme mentioned above represents the main idea for solving the equations governing mass (Eqs. (1) and (3)) and momentum (Eqs. (2) and (4)); this scheme deals with velocity-pressure coupling and avoids the numerical instability caused by high sediment concentration. The equations governing k and ϵ are also solved in "phase-intensive" forms. Other details relating to the numerical treatments are similar to "twoPhaseEulerFoam", a two-phase solver provided by OpenFOAM®.[37]

The proposed novel numerical scheme differs from those used in "twoPhaseEulerFoam" and previous two-phase models[24,40,41] mainly in the computation of $\mathbf{u}^s$ and c. The previous models compute $\mathbf{u}^s$ directly but not by prediction-correction methods. The mass balance equations in the previous models are not solved in the form similar to Eq. (29); the sediment pressure in the previous models does not appear in the mass balance equations to avoid numerical instability (see the discussion below Eq. (29)).

C. Overall solution procedure

The procedure for solving the governing equations is outlined as follows:

(1) solve Eqs. (23) and (24)
(2) compute $\mathbf{u}^{s'}$ from Eq. (27)
(3) solve Eq. (29) for c
(4) compute $\mathbf{u}^s$ from Eq. (28)
(5) compute $\mathbf{u}^{s*}$ from Eq. (33)
(6) compute $\mathbf{u}^{f*}$ from Eq. (30)
(7) solve Eq. (34) for p_f
(8) repeat (5)-(7) for n times (here, $n = 1$)
(9) compute $\mathbf{u}^f$ from Eq. (31)
(10) set $\mathbf{u}^s = \mathbf{u}^f$ for very dilute region, specifically $c \leq 10^{-6}$
(11) repeat (1)-(10) until the residuals of Eqs. (23), (29), and (34) are smaller than the tolerance (here it is 10^{-5})
(12) solve Eqs. (A4) and (A7) for k and ϵ and compute the related coefficients.

In the computations, $1/c$ is replaced by $1/(c + 10^{-6})$ to avoid singularity at $c = 0$. When c is small (say, $c \leq 10^{-6}$), the error in computing $\mathbf{u}^s$ becomes large because of the replacement. In this situation, we set $\mathbf{u}^s = \mathbf{u}^f$; this does not affect the computations of other variables because the momentum of the sediment $c\mathbf{u}^s$ for $c \leq 10^{-6}$ is very small.

When neglecting equations concerning the sediment phase, this scheme can be reduced to the "PIMPLE" scheme that is a combination of the "pressure implicit with splitting of operator" (PISO) scheme and the "semi-implicit method for pressure-linked equations" (SIMPLE) scheme. The PISO and SIMPLE schemes are widely used in fluid simulations. In this study, $n = 1$ is suggested by the SIMPLE scheme. Interactive methods are used to solve Eq. (23) for $\mathbf{u}^f$, Eq. (24) for $\mathbf{u}^s$, Eq. (29) for c, Eq. (34) for p_f, Eq. (A4) for k, and (A7) for ϵ separately; the convergence criteria are set at the residuals not exceeding 10^{-8}. Because Eqs. (23), (24), (29), and (34) are coupled, additional residual checks are performed (step 11), where convergence is achieved if residuals are less than 10^{-5}; in this study, three iterations are generally sufficient for convergence. The residual for Eq. (24) is not checked because $\mathbf{u}^s = \mathbf{u}^f$ is enforced in step (10).

The stability of the overall numerical method is restricted by the Courant–Friedrichs–Lewy (CFL) condition. The local CFL number for each cell is defined as

$$\mathrm{CFL} = \sum \frac{\mathrm{abs}\,(\mathbf{u}_i \cdot \mathbf{S}_i)}{2V} \Delta t, \tag{35}$$

where $\mathbf{u}_i = (1 - c)\,\mathbf{u}_i^f + c\mathbf{u}_i^s$, the subscript "$i$" represents the i^{th} face of the cell, $\mathbf{S}_i$ is a unit normal vector, V is the volume of the cell, and Δt is the time step. CFL is related to the ratio between the distance of a particle moving within Δt and the size of cell where such particle is located. In general, CFL < 1 is required for avoiding numerical instability. In this study, $\max\,(\mathrm{CFL}) < 0.1$ is imposed. For high concentration regions, the related CFL is desired to be much smaller than

low concentration region so that rapid changes of c are avoided; thus, $\max(\mathrm{CFL}|_{c>0.6}) < 0.005$ is imposed. The time step ranges from 10^{-5} s to 10^{-4} s in the ensuing simulations.

IV. APPLICATION TO SHEET FLOW

The proposed model is first applied to solve 1D sheet flow, a classical problem in sediment transport. Sheet flows occur when the bed shear stress τ_b is high and the Shields number $\theta = \tau_b/g(\rho_s - \rho_f)d$ exceeds at least 0.4.[42] Sediments are transported with high concentration, the sediment concentration varies gradually in space, and sand waves are washed out so that the bed flat.[43] A typical steady and uniform sheet flow is schematically plotted in Fig. 2, where h is the flow depth and δ is the thickness of the sheet flow. When θ is small, say $\theta < 0.4$, sediments transport is in its saltation regime where the sediment concentration varies rapidly near bed and much finer grid is required.

A. Test conditions

Table II lists the properties of two sediment types, A and B. Table III summarizes the four cases (1, 2, 3, and 4) studied herein; the flow conditions for Cases 1, 2, and 3 are the same as those in Runs 82, 91, and 99 in Sumer *et al.*;[43] while Case 4 corresponds to Cowen *et al.*[44] For Cases 1 to 3, u_*/w_s approaches unity while for Case 4, the value exceeds unity considerably. Hence, turbulent suspension is important in all cases. For Cases 1 to 3, $\mathrm{Re}_* > 55$, indicating that sediment inertia is important, whereas for Case 4, Re_* lies between 10 and 55, implying that both sediment inertia and fluid viscosity are prominent.

B. Numerical setup

In the x_1-direction, only one grid is used, and a periodic boundary condition is imposed. In the x_2-direction, uniform grids of length 0.5d are used. A convergence test is performed for Case 2 with a smaller grid length of 0.33d, and the discrepancies in maximum velocities are found to be within 1%. For duct flows (Cases 1-3), a wall function[45] is imposed at the top boundary, whereas shear stresses for both phases and fluxes of k and ϵ are set to be zero in the free surface flow. A no-slip boundary condition is imposed at the bottom and fluxes of k and $\epsilon = 0$ are taken. It is reiterated that the equations governing sediment (Eqs. (24) and (29)) are solved throughout the entire computational domain, including the region inside the sand bed; previous studies solve those equations only outside the sand bed. The simulation for each case takes several minutes of computational time on one thread of an Intel® Core™ i7 6700 CPU.

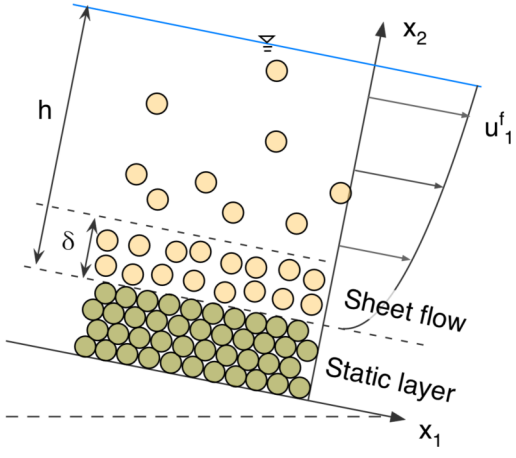

FIG. 2. Schematic diagram of sheet flow.

TABLE II. Sediment properties.

Sediment type	Composition	d (mm)	ρ_s (kg/m^3)	Fall velocity w_s (cm/s)
A	Plastic cylinder	2.6	1140	7.3
B	Sand	0.25	2600	3.26

C. Results and discussion

1. Profiles of velocities, concentrations, and pressures

The computed velocity and concentration profiles for Cases 1-3 and Case 4 are presented in Figs. 3 and 4, respectively. For Sediments A and B, $\eta_1 = 0.51$ and 0.65 respectively; the former is obtained from measurements[43] while the latter corresponds to $\theta_s = 33°$ for sands. This study takes $C_{\epsilon 3} = 1$ and 1.3 for Cases 1-3 and Case 4, respectively. The measured and computed velocities, as well as concentrations using other models[6,7,9] are also superposed in Figs. 3 and 4 for comparison. The origins of the vertical coordinates in Figs. 3 and 4 are redefined at the sand bed defined by $c = c_o$. The computed concentrations inside the sand bed are found to be very close to c_o; the differences are within 0.5%.

Figures 3(a), 3(c), and 3(e) show that the velocity profiles computed using the present model broadly agree with the measured ones by Sumer *et al.*[43] However, the present model slightly over predicts the velocity for Case 3 (Fig. 3(e)) and under predicts Case 1 (Fig. 3(a)). Since velocity is associated with bed resistance and roughness, it is deduced that the present model under predicts the bed roughness for flow with high θ but under predicts for low θ, similar to previous studies.[6] One possible explanation is that the effects of sediment on turbulence are not properly modeled. Previous studies[46,47] suggested that interaction of small particles and large turbulent eddies can attenuate turbulent kinetic energy, whereas large particles and small turbulent eddies can amplify turbulent kinetic energy; however, the present model and previous models[6,24] can only capture attenuation of turbulent kinetic energy due to the double-averaged framework mentioned in Section II A.[46,47] Some two-phase turbulence models[46,48] are available to describe the attenuation and increase of turbulence due to sediment, but these models are found to easily induce numerical instability for high concentration flows. In this study, $C_{\epsilon 2}$ and $C_{\epsilon 3}$ are taken as constants. However, Squires and Eaton[36] observed numerically that the presence of sediment can influence $C_{\epsilon 2}$ and $C_{\epsilon 3}$, although the actual mechanism is not apparent. This approximation may contribute to some of the discrepancy observed for the present model. As shown in Figs. 3(a) and 3(e), the velocity computed by the present model is slightly closer to the measured data compared to that of Hsu *et al.*[6] whose model differs from the present work mainly in the closure of sediment stress. The study of Hsu *et al.*[6] is based on granular kinetic theory but the present model is in accordance to rheological characteristics of granular materials in fluids. The drawback of using granular kinetic theory is that fluid effects on particle collision, such as the lubrication effect[49] cannot be considered.

TABLE III. Flow properties.

Case	1	2	3	4
Flow type	Duct flow	Duct flow	Duct flow	Surface flow
Energy slope	7.87×10^{-3}	9.09×10^{-3}	11.5×10^{-3}	3.5×10^{-3}
Sediment type	A	A	A	B
h(cm)	10.2	10.3	10.6	14.8
θ	1.38	1.64	2.29	1
u_*/w_s	0.96	1.05	1.23	6.5
Re$_*$	182	200	235	16

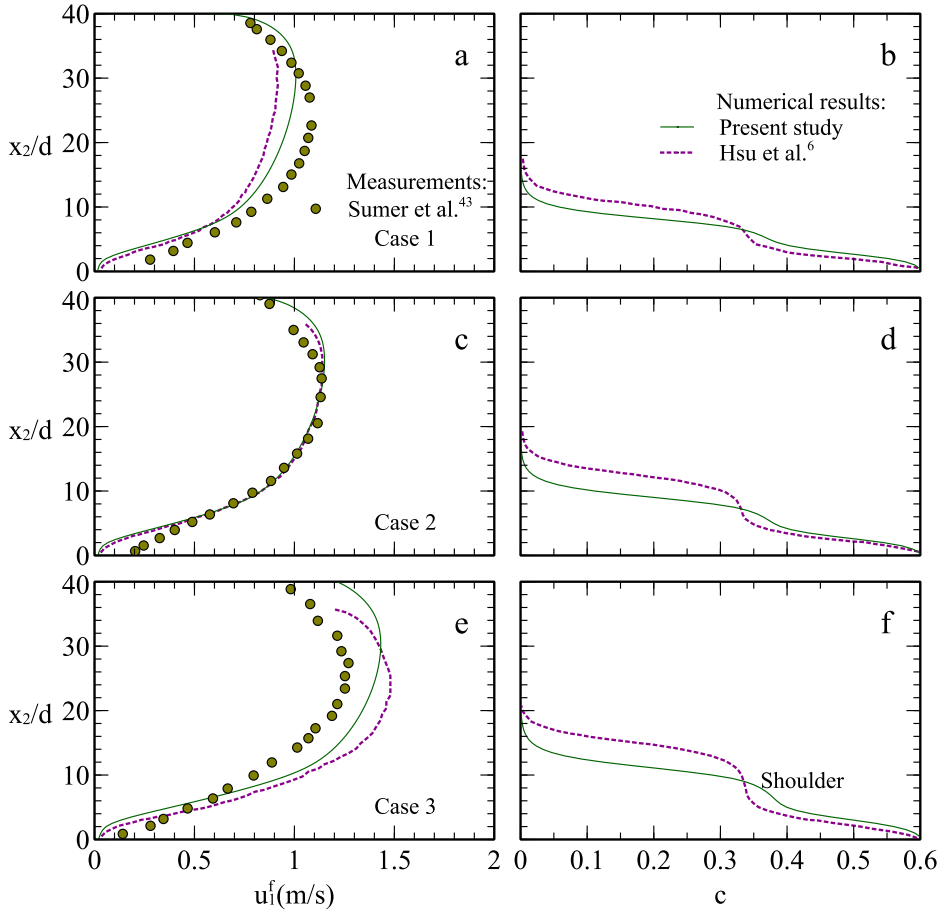

FIG. 3. Fluid velocity profile (left panel) and sediment concentration profile (right panel) for Case1 ((a) and (b)), Case 2 ((c) and (d)), and Case 3 ((e) and (f)) in Table II.

As shown in Figs. 3(b), 3(d), and 3(f), the concentration profiles computed using the two different models appear similar. The concentrations vary linearly with x_2 for $c < 0.3$ consistent with the experimental observations by Sumer *et al.*[43] for Acrylic grains. Note that concentrations for Sediment A were not measured by Sumer *et al.*,[43] and those for Acrylic grains were measured only for $c < 0.3$. The results of Hsu *et al.*[6] show concentration "shoulders" of a few particles size thickness at $c \approx 0.35$; however, there are no obvious shoulders in the present results. Capart and Fraccarollo[50] used high speed camera to measure concentration profiles of sheet flow but their

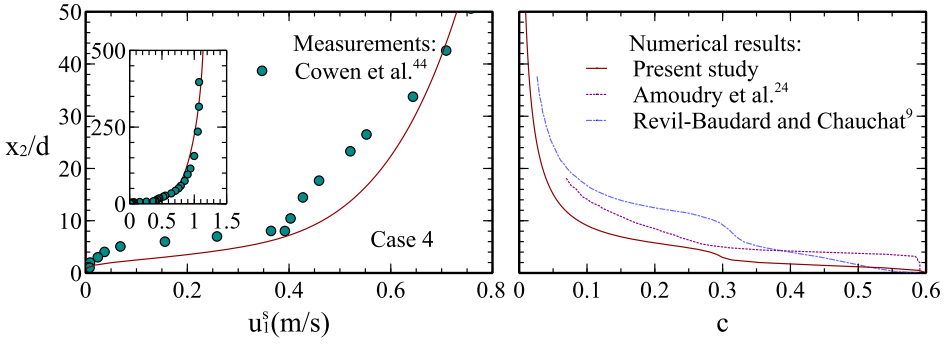

FIG. 4. Sediment velocity profile (left panel) and sediment concentration profile (right panel) for Case 4.

results (not shown here) exhibited strong near-bed fluctuations ($c > 0.35$) thus it is difficult to ascertain the presence of the shoulder.

Figure 4(a) shows that the computed velocity profile is generally consistent with measurements, but the disparity is obvious at $10 < x_2/d < 30$, where $c > 0.05$. Cowen *et al.*[44] used an acoustic Doppler velocimeter (ADV) and a borescopic quantitative imaging profiler system to measure flow velocity for $x_2/d > 10$ and $x_2/d < 10$, respectively. Since ADV is not suitable for flow velocity in high concentration region, the large deviation may be due to measurement error. As shown in Fig. 4(b), the present computed concentration is similar to Amoudry *et al.*[7] and Revil-Baudard and Chauchat.[9] The model of Amoudry *et al.*[7] is an extension of Hsu *et al.*[6] to small particles by modifying $C_{\epsilon 2}$. Similar to the present work, the work by Revil-Baudard and Chauchat[9] is also based on rheological characteristics, but a turbulence closure based on the mixing length theory is used.

Lee *et al.*[25] pointed out that using the two-phase solver provided by OpenFOAM®, called "twoPhaseEulerFoam", to simulate collapse of the granular column cannot correctly predict fluid and sediment pressures, such that the angle of repose cannot be produced. Here, the fluid and sediment pressures are computed using the proposed model. The conditions of Case 4 are imposed but with a small slope (say, 0.0001), so that sediment suspension is not obvious, and the sediment pressure will then increase linearly. The thickness of the sediment layer is about 0.05 m. The computed fluid and sediment pressures are presented in Fig. 5. Cheng and Hsu[51] modified "twoPhaseEulerFoam" slightly by using another formula to compute sediment pressure. The fluid pressure using the modified "twoPhaseEulerFoam" is also included in Fig. 5 ("twoPhaseEulerFoam" does not yield sediment pressure). The original "twoPhaseEulerFoam" is used to simulate the same case but the concentration always exceeds the random close packing fraction, which is unrealistic. In contrast, the present model can predict the correct pressures (see Fig. 5). The fluid and sediment pressures corresponding to the proposed model increase linearly toward the bed, where the slope of the fluid pressure equals the unit weight of the fluid, $\rho_f g$, and the slope of sediment pressure equals the submerged unit weight of sediment, $c(\rho_s - \rho_f)g$. Figure 5 shows that the fluid pressure from the modified "twoPhaseEulerFoam" is erroneous as it does not increase linearly.

In summary, the velocity computed by the present model agrees with the measured ones for $\mathrm{Re}_* > 55$ (sediment inertia is important) and $10 < \mathrm{Re}_* < 55$ (sediment inertia and fluid viscosity are important), suggesting that the present model is applicable for a wide range of Re_*.

2. Thickness of sheet flow and sediment transport rates

Fig. 6 plots the normalized thickness of sheet flow δ/d (defined by $c > 0.08$ suggested by Hsu *et al.*[6]) predicted by the present model for Sediments A and B. The results of Hsu *et al.*[6] and Sumer *et al.*[43] for Sediment A are included. The initial depth is 15 cm, and the free surface boundary condition is used while θ changed by varying the bed slope. It is seen in Fig. 6 that δ/d increases

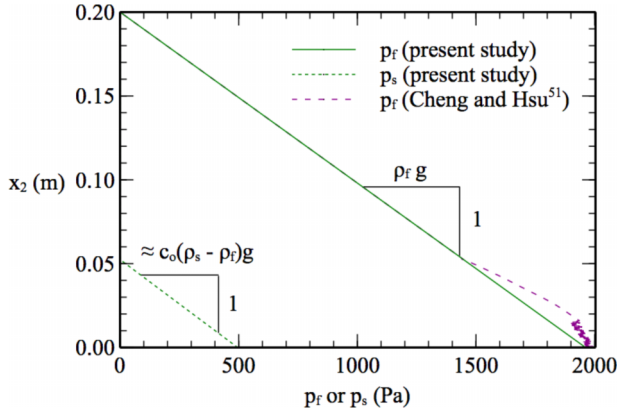

FIG. 5. Computed pressures of fluid and sediment.

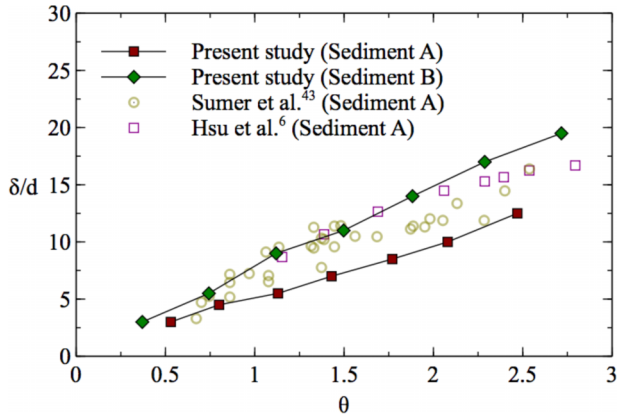

FIG. 6. Thickness of sheet flow.

with θ consistent with theoretical results.[50] The computed δ/d using the present model is smaller for Sediment A compared to Sediment B possibly because the fall velocity of Sediment A exceeds that of Sediment B (see Table II). In general, the results for Sediment A show a similar trend.

Fig. 7 plots the dimensionless sediment transport rate, $q^* = q/d\sqrt{(\rho_s/\rho_f - 1)gd}$ (where q is sediment transport rate) against θ. The bed-load transport in Fig. 7 is defined by the transport of sediment in the region with $c > 0.08$. The formulas of Meyer-Peter and Müller,[3] Ribberink,[4] and Hanes[5] are also included in figure. Meyer-Peter and Müller[3] was based on flume experiments where $d > 3$ mm and $\theta < 0.2$ while Ribberink[4] was based on laboratory experiments where d ranges from 0.2 to 3.8 mm and θ spans from 0.07 to 7. Hanes[5] was derived based on a granular fluid model for sheet flow. It is seen in Fig. 7 that the bed-load transport rates for Sediments A and B are similar with each other but the total loads exhibit significance differences. The total load for Sediment B is much larger than Sediment A possible because the fall velocity of Sediment B is smaller and is more easily suspended and transported, comparing with Sediment A. The variation tendency of the computed sediment transport rates is closer to the formula of Hanes[5] than the other two formulas.

3. Sensitivity analysis

Sensitivity analyses are performed to determine the sensitivity of the maximum fluid velocity U and the sheet flow layer thickness δ to the model parameters. Since the model parameters, c_o, c_c, c_{rcp}, χ, and K, are associated with the sediment in the static state, they are excluded in the sensitivity analyses. The flow type, sediment type, bed slope, and the depth are the same as Cowen

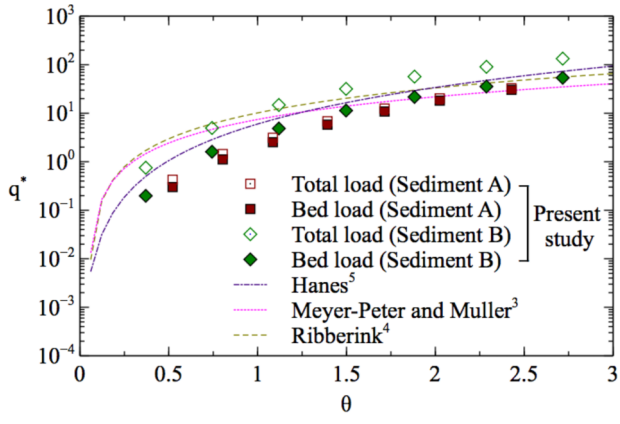

FIG. 7. Sediment transport rate versus the Shields number.

et al.[44] (see Table III); the base values for the parameters are listed in Table I; in addition, $\sigma_c = 1$, $\eta_1 = 0.65$, and $C_{\epsilon 3} = 1.3$, corresponding to $U = 1.15$ m/s and $\delta = 10d$. Table IV summarizes the ranges of the parameters and the corresponding ranges of U and δ. The ranges of a, b, η_1, and σ_c cover the values reported in the literatures: $a = 0.01 - 1$,[15,18,22] $b = 0.75 - 1$,[9,23] $I_o = 0.1 - 0.3$,[22,31] $\eta_1 = 0.49 - 0.73$,[52–55] and $1/\sigma_c = 0.25 - 2$.[27,48] Since η_2 must exceed η_1 and $\eta_2 > 1$ yields numerical instability; thus, $\eta_2 = 0.65$–1. In addition, $C_{\epsilon 3}$ may range from 1 to 4;[36] however, it is found that $C_{\epsilon 3} > 1.6$ yields numerical instability. From Table IV, it is apparent that U and δ are very sensitive to $C_{\epsilon 3}$ and σ_c. These two parameters are associated with turbulence; the former is associated with turbulence modulation and the latter with turbulent dispersion. This implies that how fluid turbulent motion and its interaction with sediment is treated is the most crucial aspect in developing a two-phase model for sediment transport. Besides, a influences U and δ—increasing a places more weight on the inertia compared to fluid viscosity when computing the sediment stresses. The significance of varying a suggests that it is essential to consider both inertial and fluid viscosity properly. Most of the previous models consider either sediment inertial or fluid viscosity. The effect of the low-Reynolds-number correction on U and δ is also examined. It is found that using low-Reynolds-number correction amplifies U by 12% and reduces δ by 26%.

V. APPLICATION TO SCOUR UNDER A PIPELINE

To study the capability of the present model for handling a multi-dimensional problem, the model is applied to simulate the scour beneath a submarine pipeline.

A. Test condition and numerical setup

Figure 8 depicts the computational domain of flow past a pipeline (of diameter D) lying on a sand layer. A backward-facing step is included in the computational domain, leading to scour occurring near the step, and a hill forming and moving downstream; thus, the results presented hereafter are before the time that the hill reaches the scour hole beneath the pipeline. The simulation parameters are $h = 23$ cm, $D = 5$ cm, $d = 0.36$ mm, $\rho_s = 2600$ kg/m^3, and mean velocity $\overline{U} = 0.87$ m/s identical to those used in the experiments of Mao.[56] A typical value of $\eta_1 = 0.65$ for sand is taken. For the fitting parameter, it is found that $C_{\epsilon 3} = 1$ provides the best fit to measured scour depths. The Shields number far from the pipeline, θ_∞, is 0.33 close to $\theta = 0.4$ for the sheet flow analysis in Section IV. In other available cases of Mao,[56] θ_∞ is much smaller than 0.4; those conditions are thus not suitable for the present analysis. Previous studies based on the single-phase approach[57] and two-phase approach[21] simulate only the cases of Mao[56] with $\theta \ll 0.4$, hence the present results are not compared to previous numerical studies.

A hydraulically rough flow of clear water with logarithmic velocity profile[58] and roughness = 2.5 d is specified at the inlet; $\overline{U}$ at the inlet increases linearly from 0 to 0.87 m/s within 4 s. In addition, $k = 10^{-4}\overline{U}$ and $\epsilon = k^{1.5}/0.1h$ are adopted.[45] The normal gradients of all parameters are

TABLE IV. Summary of sensitivity analysis on sheet flow. The base values correspond to $U = 1.15$ m/s and $\delta = 10\ d$.

Varying parameter	Varying ranges	U (m/s)	δ (d)
a	0, 0.11, 1	1.57 → 0.92 (71%)	7.5 → 13 (73%)
b	0.5, 1, 1.5	1.3 → 1.04 (25%)	8.5 → 11 (29%)
I_o	0, 0.1, 0.3	1.11 → 1.17 (5%)	10
η_1	0.45, 0.65, 0.75	1.26 → 1.09 (16%)	11 → 8.5 (29%)
η_2	0.65, 0.82, 1	1.29 → 1.03 (25%)	10
$C_{\epsilon 3}$	1, 1.3, 1.6	2.11 → 0.87 (143%)	8.5 → 27 (218%)
$1/\sigma_c$	0, 1, 2	0.6 → 1.48 (146%)	3 → 13 (333%)

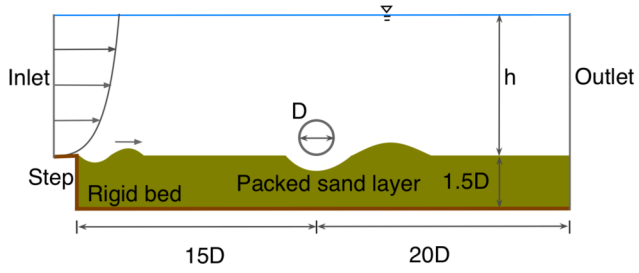

FIG. 8. Schematic diagram of flow past a pipeline.

zero at the outlet except for fluid pressure. On the free surface, flow is assumed to be symmetric. A wall-function boundary condition for smooth wall[45] is imposed on the cylinder surface and the same for rough wall is specified on the rigid bed. The fluid pressure is given by the hydrostatic pressure at the outlet. On other boundaries, the OpenFOAM® build-in function "fixFluxPressure" is imposed that adjust the pressure gradient to make the governing equations of momentum holds on the boundaries. The computational domain is divided into numerous unstructured quadrilateral cells, as shown in Fig. 9, using OpenFOAM® built-in functions, i.e., "blockMesh" and "snappyHexMesh". The smallest grid for the packed sand layer is of height $1.7d$; further refinement is not considered due to prohibitive computational cost (Amoudry and Liu[24] used a grid height of $4d$ in scour simulations). A convergence test is performed for the 2D case with coarse grid height of $3.4d$. The discrepancy in the scour hole depth at $t = 11$ s is found to be 4% with the more refined grid having better agreement with measurements. The computational time for the pipeline scour problem is about four days to simulate 32 s of the scour process, using six threads on an Intel® Core™ i7 6700 CPU. It can be seen in Eq. (32) that $\nabla \cdot \mathbf{u} = 0$ with $\mathbf{u} = (1 - c)\,\mathbf{u}^f + c\boldsymbol{u}^s$. In the simulation, the summation of $|\nabla \cdot \mathbf{u}|V\Delta t$ in the whole domain for each time step is within 2×10^{-10} m^3, which is very small compared to the domain size of about 0.02 m^3.

B. Results and discussion

Figure 10 portrays the bed evolution around the pipeline. Since the proposed two-phase model simulates the sediment concentration, the bed profile is not explicit and needs to be defined. Here, it is delineated by $c = 0.5$, which yields similar bed profiles with $c = c_o$ as in Section IV. It is

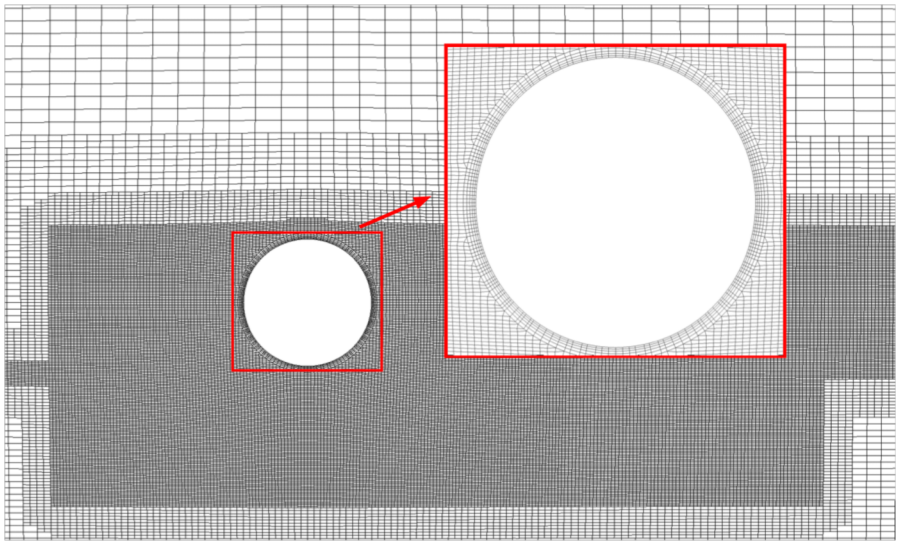

FIG. 9. Mesh in the vicinity of the pipeline.

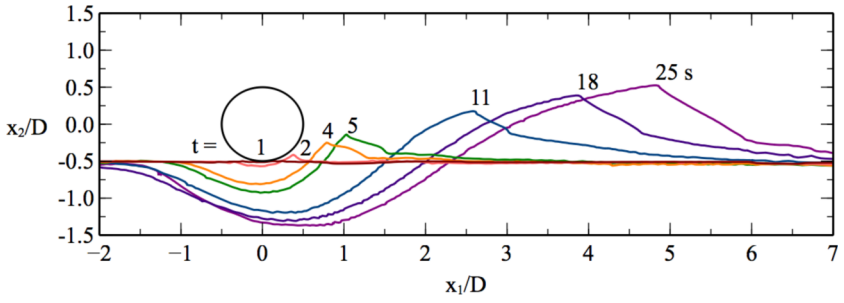

FIG. 10. Time evolution of the bed profile.

apparent from Fig. 10 that the onset of scour occurs between 1 s and 2 s. The onset of scour occurs when the seepage flow, induced by large pressure difference between upstream and downstream of the pipeline, washes out the sediments beneath the pipeline.[59] Previous numerical models, whether single-phase[57] or two-phase,[21] cannot simulate the onset of scour and an initial gap between the sand layer and pipeline is required. Since the onset of scour is a 3D phenomenon[60] and only 2D simulation is performed here, this paper will not focus on it. After the onset, the scour hole enlarges in depth and width with time while the hill forms behind the pipeline and grows over time consistent with Mao's[56] observations.

Figure 11 plots the evolution of S/D, where S is the maximum scour depth; the data of Mao[56] are superposed for comparison. Both curves increase with time and approach similar equilibrium values. In general, there is a good agreement between the computed and measured scour depths thus validating the present model. However, some bumps are observed in the computed curve, for instance at $t = 23$ s, because of small sand ripples forming and migrating in front of the pipeline. Moreover, the computed scour rate $\mathrm{d}S/\mathrm{d}t$ is more rapid compared to measurements for $t < 4$ s. This disparity may be attributed to the difference in the flow field at $t = 0$. More specifically, in the simulations, zero velocity is assumed for the initiate state, consequently the vortex behind the pipeline has not fully developed at $t < 4$ s.

The scour process also includes two other stages: one is jet scour,[56] also known as tunnel erosion,[61] and the other is lee-wake erosion.[61] Tunnel erosion occurs in the early stages when the gap between the pipeline and bed is small, say $S/D < 0.3$.[56] In this stage, a large amount of fluid is diverted into the gap, forming a jet beneath the pipeline and causing large fluid velocities and large shear stress on the bed. Lee-wake erosion occurs when $S/D > 0.3$ and vortex shedding from the pipeline has strong tendency to move sediment away.[56] Figure 12 illustrates the computed flow field at $t = 4$ s and 11 s. The scour process at $t = 4$ s is classified as tunnel erosion since $S/D \approx 0.3$ (see Fig. 11), and lee-wake erosion occurs at $t = 11$ s because $S/D > 0.3$. A jet is observed at $t = 4$ s

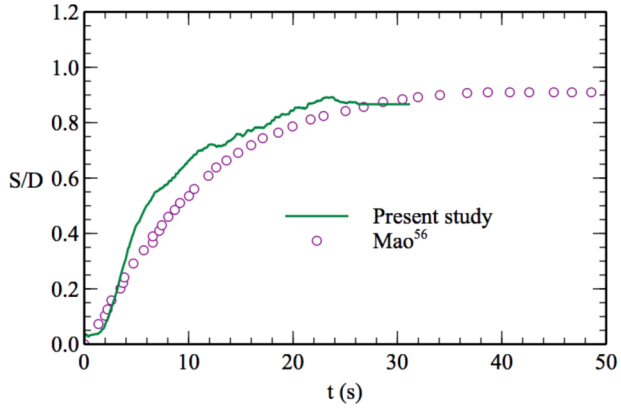

FIG. 11. Time development of scour depth.

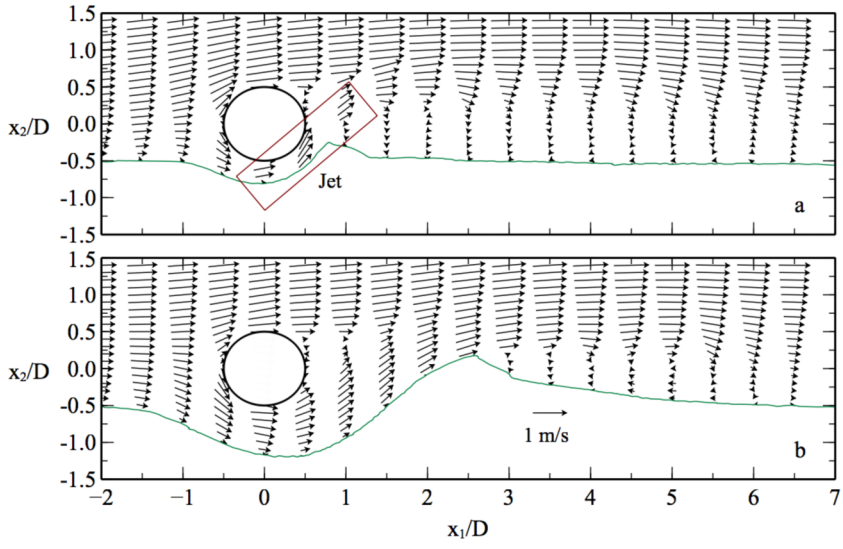

FIG. 12. Computed fluid velocity at $t = 4$ s (a) and 11 s (b).

and a vortex forms behind the hill consistent with Mao;[56] however, no vortex shedding is observed at $t = 11$ s possibly because of the $k - \epsilon$ model. Prior researchers[62,63] have also suggested that the $k - \epsilon$ model fails to capture vortex shedding although it can produce accurate mean flow field. In principle, this shortcoming can be overcome by switching to other turbulence models, such as $k - \omega$ models;[64,65] however, for the two-phase model, there are other unresolved challenges, such as how the sediment effect can be incorporated into ω.

Figures 13 and 14 plot the sediment concentration and velocity, respectively. The measured bed profile at $t = 11$ s is also superposed in Fig. 13 (the profile at $t = 4$ s is unavailable). Around the pipeline, the sediments are washed out and leave the bed from the crest of the hill; subsequently, the sediments are deposited behind the hill. Some sediments downstream of the hill ($3 < x_1/D < 6$) move upstream due to the vortex (see Fig. 12), as observed experimentally.[56] The iso-concentration line of $c = 0.5$ agree with the measured bed profile except that the computed hill

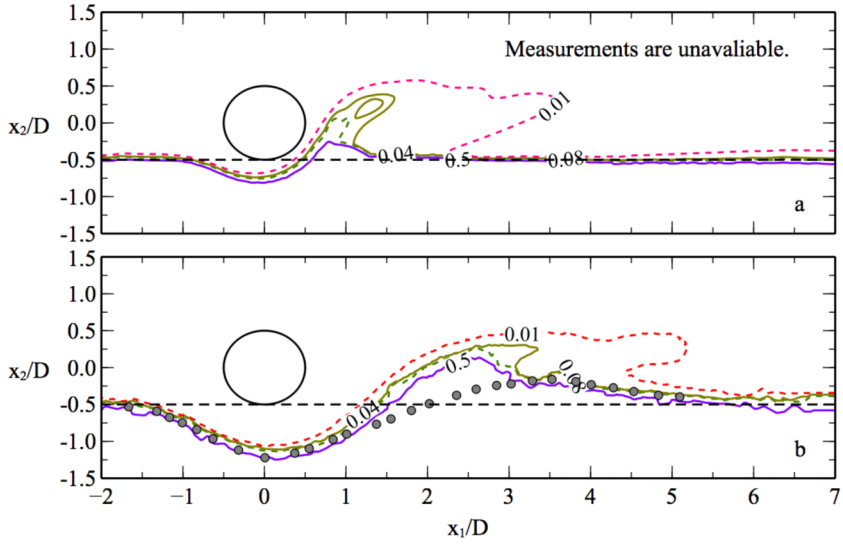

FIG. 13. Computed sediment concentrations (lines) and measured bed profiles by Mao[56] (circles) at $t = 4$ s (a) and 11 s (b).

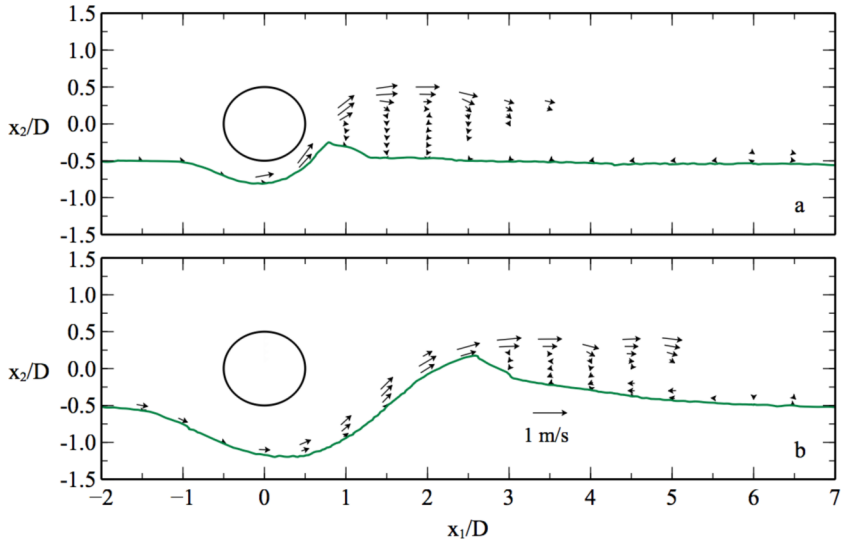

FIG. 14. Computed sediment velocity at $t = 4$ s (a) and 11 s (b) in the region with $c \geq 0.01$.

(at $1.5 < x_1/D < 3$) is more prominent than the measured one; one possible explanation is that vortex shedding is not properly captured.

The successful application of the present model to simulate scour under a pipeline demonstrates the capability of the present model to solve multi-dimensional problems. However, due to failure in simulating the vortex shedding, the computed bed elevations may be overestimated in locations where vortex shedding is pronounced.

C. Sensitivity analysis

Table V summarizes the analysis of the sensitivity of S/D and the height of the hill behind the pipeline H, at $t = 11$ s, to the model parameters. The ranges of the model parameters are the same as those in Table IV. The base values for the model parameters are listed in Table I. In addition, $\sigma_c = 1$, $\eta_1 = 0.65$, and $C_{\epsilon 3} = 1$, leading to $S/D = 0.7$ and $H/D = 0.68$. It is not surprising that S and H are highly sensitive to $C_{\epsilon 3}$ and σ_c given that these parameters are highly influential for sheet flow (see Section IV C 3).

TABLE V. Summary of sensitivity analysis on S/D and H/D at $t = 11$ s. The base values correspond to $S/D = 0.7$ and $H/D = 0.68$.

Varying parameter	Values	S/D	H/D
a	0, 0.11, 1	0.67 → 0.7 (4%)	0.64 → 0.7 (9%)
b	0.5, 1, 1.5	0.68-0.7 (3%)	0.66 → 0.69 (5%)
I_o	0, 0.1, 0.3	0.69 → 0.67 (3%)	0.68
η_1	0.45, 0.65, 0.75	0.69-0.7 (1%)	0.66-0.68 (3%)
η_2	0.65, 0.82, 1	0.69-0.7 (2%)	0.68
$C_{\epsilon 3}$	1, 1.3, 1.6	0.7 → 0.83 (19%)	0.68 → 0.58 (17%)
$1/\sigma_c$	0, 1, 2	0.61-0.7 (15%)	0.7 → 0.58 (20%)

VI. CONCLUSIONS

This paper outlines the development of a new numerical model for sediment transport. The salient features of the proposed model are as follows:

(1) Two-phase approach, enabling the fluid-sediment interaction and inter-sediment interaction to be rigorously modeled, which is not feasible for the widely used single-phase approaches.[1,2]
(2) Rheological characteristics[22,23] recently published are incorporated, permitting the model to be applicable to a wide range of Re_*, as both fluid viscosity and sediment inertia effects are included in computing the sediment stress. Previous studies generally do not consider both two effects simultaneously except for two models[9,15] that are limited to 1D problems.
(3) Three-dimensional unlike most previous studies that are constrained to 1D applications. Two previous models[21,24] are 2D but use structured grid systems. The present model supports unstructured grids and is thereby more versatile.
(4) Novel numerical scheme that prevents numerical instability in high concentration region, allowing the entire domain to be solved numerically. In contrast, previous 2D models[21,24] simulate only the region outside the sand bed, assuming that sediments within the sand bed are static.

The present model is applied to two classical problems—sheet flow and scour under a pipeline—with favorable results. For sheet flow, the computed velocity profiles agree well with measured ones reported in the literature. Besides, the sediment transport rates and the computed sheet flow thicknesses are close to that obtained in previous studies. For scour under a pipeline, the computed scour depth development matches previous experimental observations.[56] Sensitivity studies are performed, and the computed results are found to be sensitive to model parameters associated with effect of sediment on turbulence.

The present model still has certain shortcomings. There is a fitting parameter $C_{\epsilon 3}$ related to sediment effect on turbulence and so far it has not been well studied in the literature. In addition, for the pipeline scour problem, the sediment deposition behind the pipeline is overestimated. One possible reason is that the present model is unable to capture vortex shedding due to the $k-\epsilon$ turbulence model adopted. The present model can potentially be improved by using other turbulence models.

Finally, it is mentioned that the new techniques developed in this paper are of a fundamental nature, and with suitable modifications, they may potentially be applied to other solid-liquid flow problems, such as debris flows, avalanches, underwater landslide, and turbidity currents.

ACKNOWLEDGMENTS

The authors gratefully acknowledge the financial support provided by the Singapore Maritime Institute (SMI) and EMAS AMC, under the SMI Deepwater Technology R&D Programme (Research Grant Number SMI-2014-OF-12).

APPENDIX: CONSTITUTIVE EQUATIONS FOR FLUID STRESSES

In this study, $\mathbf{T}^{fv}$ is computed by

$$\mathbf{T}^{fv} = -\rho_f \left(\frac{2}{3} \nu_f \nabla \cdot \mathbf{u}^f \right) \mathbf{I} + 2\rho_f \nu_f \mathbf{D}^f, \tag{A1}$$

where ν_f is the kinematic viscosity of fluid and $\mathbf{D}^f = \left[\nabla \mathbf{u}^f + \left(\nabla \mathbf{u}^f \right)^T \right] /2$. Some previous studies[9] suggested modifying ν_f to consider sediment effect; however, other studies[15] neglected this effect and still obtained satisfactory results. Consequently, in this work, ν_f is regarded as a constant ($10^{-6}\,\mathrm{m}^2/\mathrm{s}$).

As in the $k-\epsilon$ model of Launder and Sharma[28] with low-Reynolds-number correction, $\mathbf{T}^{ft}$ is computed using

$$\mathbf{T}^{ft} = -\rho_f \left(\frac{2}{3}k + \frac{2}{3}\nu_{ft}\nabla\cdot\mathbf{u}^f\right)\mathbf{I} + 2\rho_f\nu_{ft}\mathbf{D}^f, \tag{A2}$$

where k is the turbulence kinetic energy and ν_{ft} is the eddy viscosity given by

$$\nu_{ft} = f_\mu C_\mu k^2/\epsilon, \tag{A3}$$

where $f_\mu = \exp[-3.4/(1+\mathrm{Re}_t/50)^2]$ represents the low-Reynolds-number correction with $\mathrm{Re}_t = k^2/\nu_f\epsilon$ and C_μ is a constant. The equations governing k that is solved herein is similar to previous studies,[6,8] i.e.,

$$\begin{aligned}\frac{\partial\rho_f(1-c)k}{\partial t} + \nabla\cdot\left[\rho_f(1-c)\mathbf{u}^f k\right] &= (1-c)\mathbf{T}^f:\nabla\mathbf{u}^f - \rho_f(1-c)\epsilon \\ &+ \nabla\cdot\left[\rho_f\frac{\nu_{ft}}{\sigma_k}(1-c)k\right] - (\rho_s-\rho_f)\frac{(1-c)\nu_{ft}}{\sigma_k}\nabla c\cdot\mathbf{g} \\ &- \frac{2\rho_s c(1-\alpha)k}{\tau_p},\end{aligned} \tag{A4}$$

where σ_k is an empirical coefficient and

$$\alpha = \frac{\tau_l}{\tau_l + \min(\tau_p,\tau_c)} \tag{A5}$$

with $\tau_l = 0.165k/\epsilon$ being the time scale of turbulent flow and τ_c the time scale of particle collisions. The last two terms of Eq. (A4) account for the effect of sediment particle on dissipation of k (turbulence modulation); the former is due to buoyance and the latter is associated with the correlation of sediment fluctuating velocity and fluid fluctuating velocity.[8] Equation (A5) is used by Hsu *et al.*[6] and Kranenburg *et al.*[8] proposed an alternative formula to compute α, which does not include τ_c, and obtained smaller turbulence decay compared with Eq. (A5). It is found that using the formula of Kranenburg *et al.*[8] yields too much sediment suspension in the pipeline scour problem. In Hsu *et al.*,[6] τ_c is a function of the sediment concentration and the fluctuating energy of sediment. However, the fluctuating energy is not available in this study, thus τ_c is taken as the inertial time of sediment rearrangement[66] with a correction for sediment concentration, i.e.,

$$\tau_c = \left[\left(\frac{c_{rcp}}{c}\right)^{\frac{1}{3}} - 1\right] d\left(\frac{\rho_s}{p}\right)^{1/2}, \tag{A6}$$

where c_{rcp} = random close packing fraction. The term $\left(c_{rcp}/c\right)^{1/3} - 1$ is related to the ratio of mean free dispersion distance to the granular diameter.[18] The equations governing ϵ are similar to previous studies[6,8] but include additional damping terms

$$\begin{aligned}&\frac{\partial\rho_f(1-c)\epsilon}{\partial t} + \nabla\cdot\left[\rho_f(1-c)\mathbf{u}^f\epsilon\right] \\ &= \frac{\epsilon}{k}\left[C_{\epsilon1}f_1(1-c)\mathbf{T}^f:\nabla\mathbf{u}^f - C_{\epsilon2}f_2\rho_f(1-c)\epsilon - C_{\epsilon3}(\rho_s-\rho_f)\frac{(1-c)\nu_{ft}}{\sigma_k}\nabla c\cdot\mathbf{g}\right. \\ &\left. - C_{\epsilon3}\frac{2\rho_s c(1-\alpha)k}{\tau_p}\right] + \nabla\cdot\left[\rho_f\frac{\nu_{ft}}{\sigma_\epsilon}(1-c)\epsilon\right],\end{aligned} \tag{A7}$$

where $C_{\epsilon1}$, $C_{\epsilon2}$, $C_{\epsilon3}$, and σ_ϵ are empirical coefficients while $f_1 = 1$ and $f_2 = 1 - 0.3\exp(-\mathrm{Re}_t^2)$ are for the low-Reynolds-number correction.[28] Because there are no available studies relating to sediment effect on these parameters, C_μ, $C_{\epsilon1}$, $C_{\epsilon2}$, σ_k, and σ_ϵ are assumed to be identical to the models for clear water.

[1] N. G. Jacobsen, J. Fredsoe, and J. H. Jensen, "Formation and development of a breaker bar under regular waves. Part 1: Model description and hydrodynamics," Coastal Eng. **88**, 182 (2014).
[2] X. F. Liu and M. H. Garcia, "Three-dimensional numerical model with free water surface and mesh deformation for local sediment scour," J. Waterw. Port Coastal Ocean Eng. **134**, 203 (2008).
[3] E. Meyer-Peter and R. Müller, "Formulas for bed-load transport," in *Proceedings of 2nd Meeting International Association for Hydraulic Research* (International Association of Hydraulic Research, Stockholm, Sweden, 1948), p. 39.
[4] J. S. Ribberink, "Bed load transport for steady and unsteady oscillatory flow," Coastal Eng. **34**, 59 (1998).
[5] D. M. Hanes, "Grain flows and bed-load sediment transport: Review and extension," Acta Mech. **63**, 131 (1986).
[6] T.-J. Hsu, J. T. Jenkins, and P. L.-F. Liu, "On two-phase sediment transport: Sheet flow of massive particles," Proc. R. Soc. A **460**, 2223 (2004).
[7] L. Amoudry, T. J. Hsu, and P. L. F. Liu, "Two-phase model for sand transport in sheet flow regime," J. Geophys. Res. **113**, C03011, doi:10.1029/2007JC004179 (2008).
[8] W. M. Kranenburg, T.-J. Hsu, and J. S. Ribberink, "Two-phase modeling of sheet-flow beneath waves and its dependence on grain size and streaming," Adv. Water Resour. **72**, 57 (2014).
[9] T. Revil-Baudard and J. Chauchat, "A two-phase model for sheet flow regime based on dense granular flow rheology," J. Geophys. Res. **118**, 619, doi:10.1029/2012jc008306 (2013).
[10] H. Liu and S. Sato, "A two-phase flow model for asymmetric sheetflow conditions," Coastal Eng. **53**, 825 (2006).
[11] H. M. Kazeminezhad, A. Yeganeh-bakhtiary, A. Etemad-Shahidi, and J. H. Baas, "Two-phase simulation of wave-Induced tunnel scour beneath marine pipelines," J. Hydraul. Eng. **138**, 517 (2011).
[12] X. Chen, Y. Li, X. Niu, M. Li, D. Chen, and X. Yu, "A general two-phase turbulent flow model applied to the study of sediment transport in open channels," Int. J. Multiphase Flow **37**, 1099 (2011).
[13] L. Li and M. Sawamoto, "Multi-phase model on sediment transport in sheet-flow regime under oscillatory flow," Coastal Eng. Jpn. **38**, 157 (1995).
[14] S. B. Pope, *Turbulent Flows* (Cambridge University Press, New York, 2000).
[15] F. Chiodi, P. Claudin, and B. Andreotti, "A two-phase flow model of sediment transport: Transition from bedload to suspended load," J. Fluid Mech. **755**, 20 (2014).
[16] X. Chen, Y. Li, X. J. Niu, D. Y. Chen, and X. P. Yu, "A two-phase approach to wave-induced sediment transport under sheet flow conditions," Coastal Eng. **58**, 1072 (2011).
[17] C. S. Campbell, "Granular material flows—An overview," Powder Technol. **162**, 208 (2006).
[18] R. A. Bagnold, "Experiments on a gravity-free dispersion of large solid spheres in a Newtonian fluid under shear," Proc. R. Soc. A **225**, 49 (1954).
[19] C.-H. Lee and C.-J. Huang, "Model of sheared granular material and application to surface-driven granular flows under gravity," Phys. Fluids **22**, 43307 (2010).
[20] C.-H. Lee and C.-J. Huang, "Kinetic-theory-based model of dense granular flows down inclined planes," Phys. Fluids **24**, 73303 (2012).
[21] A. Yeganeh-Bakhtiary, M. H. Kazeminezhad, A. Etemad-Shahidi, J. H. Baas, and L. Cheng, "Euler–Euler two-phase flow simulation of tunnel erosion beneath marine pipelines," Appl. Ocean Res. **33**, 137 (2011).
[22] M. Trulsson, B. Andreotti, and P. Claudin, "Transition from the viscous to inertial regime in dense suspensions," Phys. Rev. Lett. **109**, 118305 (2012).
[23] F. Boyer, E. Guazzelli, and O. Pouliquen, "Unifying suspension and granular rheology," Phys. Rev. Lett. **107**, 188301 (2011).
[24] L. O. Amoudry and P. L.-F. Liu, "Two-dimensional, two-phase granular sediment transport model with applications to scouring downstream of an apron," Coastal Eng. **56**, 693 (2009).
[25] C.-H. Lee, Z. Huang, and Y.-M. Chiew, "A three-dimensional continuum model incorporating static and kinetic effects for granular flows with applications to collapse of a two-dimensional granular column," Phys. Fluids **27**, 113303 (2015).
[26] D. A. Drew, "Mathematical modeling of two-phase flow," Annu. Rev. Fluid Mech. **15**, 261 (1983).
[27] T.-J. Hsu and P. L. F. Liu, "Toward modeling turbulent suspension of sand in the nearshore," J. Geophys. Res. **109**, C06018, doi:10.1029/2003jc002240 (2004).
[28] B. E. Launder and B. I. Sharma, "Application of the energy-dissipation model of turbulence to the calculation of flow near a spinning disc," Lett. Heat Mass Transfer **1**, 131 (1974).
[29] S. Chialvo, J. Sun, and S. Sundaresan, "Bridging the rheology of granular flows in three regimes," Phys. Rev. E **85**, 21305 (2012).
[30] J. Hinze, *Turbulence* (McGraw Hill, New York, 1959).
[31] P. Jop, Y. Forterre, and O. Pouliquen, "A constitutive law for dense granular flows," Nature **441**, 727 (2006).
[32] R. M. Iverson, "The physics of debris flows," Rev. Geophys. **35**, 245, doi:10.1029/97RG00426 (1997).
[33] C. Cassar, M. Nicolas, and O. Pouliquen, "Submarine granular flows down inclined planes," Phys. Fluids **17**, 103301 (2005).
[34] J. Chauchat and M. Médale, "A three-dimensional numerical model for dense granular flows based on the μ(I) rheology," J. Comput. Phys. **256**, 696 (2014).
[35] O. Pouliquen, C. Cassar, P. Jop, Y. Forterre, and M. Nicolas, "Flow of dense granular material: Towards simple constitutive laws," J. Stat. Mech. **2006**, P07020 (2006).
[36] K. D. Squires and J. K. Eaton, "Effect of selective modification of turbulence on two-equation models for particle-laden turbulent flows," J. Fluids Eng. **116**, 778 (1994).
[37] H. Rusche, "Computational fluid dynamics of dispersed two-phase flows at high phase fractions," Ph.D. thesis, University of London, London, 2003.
[38] W. T. Hancox and S. Banerjee, "Numerical standards for flow-boiling analysis," Nucl. Sci. Eng. **64**, 106 (1977).
[39] M. B. Carver, "Numerical computation of phase separation in two fluid flow," J. Fluids Eng. **106**, 147 (1984).
[40] R. Bakhtyar, D. A. Barry, A. Yeganeh-Bakhtiary, L. Li, J. Y. Parlange, and G. C. Sander, "Numerical simulation of two-phase flow for sediment transport in the inner-surf and swash zones," Adv. Water Resour. **33**, 277 (2010).
[41] A. D. Gosman, C. Lekakou, S. Politis, R. I. Issa, and M. K. Looney, "Multidimensional modeling of turbulent two-phase flows in stirred vessels," AIChE J. **38**, 1946 (1992).

[42] S. Wang and W. R. White, "Alluival resistance in transition regime," J. Hydraul. Eng. **119**, 725 (1993).
[43] B. M. Sumer, A. Kozakiewicz, J. Fredsøe, and R. Deigaard, "Velocity and concentration profiles in sheet-flow layer of movable bed," J. Hydraul. Eng. **122**, 549 (1997).
[44] E. A. Cowen, R. D. Dudley, Q. Liao, E. A. Variano, and P. L.-F. Liu, "An in situ borescopic quantitative imaging profiler for the measurement of high concentration sediment velocity," Exp. Fluids **49**, 77 (2010).
[45] J. H. Ferziger and M. Peric, *Computational Methods for Fluid Dynamics* (Springer, Berlin, 2002).
[46] C. T. Crowe, "On models for turbulence modulation in fluid–particle flows," Int. J. Multiphase Flow **26**, 719 (2000).
[47] C. T. Crowe, T. R. Troutt, J. N. Chung, R. Troutt, and N. Chung, "Numerical models for two-phase turbulent flows," Annu. Rev. Fluid Mech. **28**, 11 (1996).
[48] C.-H. Lee, Z. Huang, and Y.-M. Chiew, "A multi-scale turbulent dispersion model for dilute flows with suspended sediment," Adv. Water Resour. **79**, 18 (2015).
[49] X. Li, M. L. Hunt, and T. Colonius, "A contact model for normal immersed collisions between a particle and a wall," J. Fluid Mech. **691**, 123 (2012).
[50] H. Capart and L. Fraccarollo, "Transport layer structure in intense bed-load," Geophys. Res. Lett. **38**, L20402, doi:10.1029/2011GL049408 (2011).
[51] Z. Cheng and T.-J. Hsu, "A multi-dimensional two-phase Eulerian model for sediment transport," Research Report No. CACR-14-08, Center for Applied Coastal Research, University of Delaware, 2014.
[52] D. B. Simons and M. L. Albertson, "Uniform water conveyance channels in alluvial materials," J. Hydraul. Div. **86**, 33 (1960).
[53] P. Nielsen, *Coastal Bottom Boundary Layers and Sediment Transport* (World Scientific, Singapore, 1992).
[54] D. M. Hanes and D. L. Inman, "Experimental evaluation of a dynamic yield criterion for granular fluid flows," J. Geophys. Res. **90**, 3670, doi:10.1029/JB090iB05p03670 (1985).
[55] J. M. Sperry and J. J. Peirce, "A model for estimating the hydraulic conductivity of granular material based on grain shape, grain size, and porosity," Ground Water **33**, 892 (1995).
[56] Y. Mao, *The Interaction Between a Pipeline and An Erodible Bed*, Series Paper (Technical University of Denmark, 1987).
[57] D. Liang, L. Cheng, and F. Li, "Numerical modeling of flow and scour below a pipeline in currents: Part II. Scour simulation," Coastal Eng. **52**, 25 (2005).
[58] M. H. García, *Sedimentation Engineering: Processes, Measurements, Modeling, and Practice* (ASCE Publications, New York, 2008).
[59] Y. M. Chiew, "Mechanics of local scour around submarine pipelines," J. Hydraul. Eng. **116**, 515 (1990).
[60] B. M. Sumer, C. Truelsen, T. Sichmann, and J. Fredsøe, "Onset of scour below pipelines and self-burial," Coastal Eng. **42**, 313 (2001).
[61] B. M. Sumer and J. Fredsøe, *The Mechanics of Scour in the Marine Environment* (World Scientific Publishing Co Pte Ltd., Singapore, 2002).
[62] M. S. Kirkgoz, A. A. Oner, M. S. Akoz, M. Salih Kirkgoz, and M. Sami Akoz, "Numerical modeling of interaction of a current with a circular cylinder near a rigid bed," Adv. Eng. Software **40**, 1191 (2009).
[63] D. Liang and L. Cheng, "Numerical modeling of flow and scour below a pipeline in currents. Part I. Flow simulation," Coastal Eng. **52**, 25 (2005).
[64] F. R. Menter, "Improved two-equation K-Omega turbulence models for aerodynamic flows," NASA STI/Recon Technical Report No. TM-103975, 1992.
[65] D. C. Wilcox, "Formulation of the k-w turbulence model revisited," AIAA J. **46**, 2823 (2008).
[66] F. Boyer, O. Pouliquen, and E. Guazzelli, "Dense suspensions in rotating-rod flows: Normal stresses and particle migration," J. Fluid Mech. **686**, 5 (2011).